International Journal of Nanomedicine

Dovepress
open access to scientific and medical research

Open Access Full Text Article

ORIGINAL RESEARCH

Ultrasound-Targeted Microbubble Disruption with Key Nanodroplets for Effective Ferroptosis in Triple-Negative Breast Cancer Using Animal Model

Rui Liu, Dandan Shi, Lu Guo, Shan Xiao, Mengmeng Shang, Xiao Sun, Dong Meng, Yading Zhao, Xiaoxuan Wang, Jie Li

Department of Ultrasound, Qilu Hospital of Shandong University, Jinan, Shandong, 250012, People's Republic of China

Correspondence: Jie Li, Department of Ultrasound, Qilu Hospital of Shandong University, Jinan, Shandong, 250012, People's Republic of China, Email jieli@email.sdu.edu.cn

Introduction: Triple-negative breast cancer (TNBC) is known to be the most aggressive form of breast cancer. Due to its high recurrence and mortality rates, the treatment of TNBC is a significant challenge for the medical community. Besides, ferroptosis is an emerging regulatory cell death that may provide new insights into the treatment of TNBC. As a central inhibitor of the ferroptosis process, the selenoenzyme glutathione peroxidase 4 (GPX4) is its classical therapeutic target. However, inhibition of GPX4 expression is quite detrimental to normal tissues. Ultrasound contrast agents, as an emerging visualization precision treatment, may provide a solution to the existing problem.

Methods: In this study, nanodroplets (NDs) carrying simvastatin (SIM) were constructed using the homogeneous/emulsification method. Then, the characterization of SIM-NDs was systematically evaluated. Meanwhile, in this study, the ability of SIM-NDs combined with ultrasound-targeted microbubble disruption (UTMD) to initiate ferroptosis and its respective mechanisms of ferroptosis induction were verified. Finally, the antitumor activity of SIM-NDs was investigated in vitro and in vivo using MDA-MB-231 cells and TNBC animal models.

Results: SIM-NDs exhibited excellent pH- and ultrasound-responsive drug release and noticeable ultrasonographic imaging ability, also showing good biocompatibility and biosafety. UTMD could promote increased intracellular reactive oxygen species and consume intracellular glutathione. However, SIM-NDs were efficiently internalized into cells under ultrasound irradiation, followed by the rapid release of SIM, which inhibited intracellular mevalonate production, and synergistically downregulated GPX4 expression, thereby promoting ferroptosis. Moreover, this combined treatment demonstrated strong antitumor ability in vitro and in vivo.

Conclusion: The combination of UTMD and SIM-NDs presents a promising avenue for harnessing ferroptosis in the treatment of malignant tumors.

Keywords: ultrasound-targeted microbubble disruption, nanodroplets, ferroptosis, glutathione peroxidase 4, theranostics, lipid peroxidation

Introduction

Breast cancer is the most common diagnosed cancer in women and also the leading cause of cancer death. Triple-negative breast cancer (TNBC) is the most aggressive type of breast cancer, occupying 10% to 20% of all cases.[1] Due to the absence of the estrogen receptor, progesterone receptor, and human epidermal growth factor receptor 2 (HER2) in TNBC patients,[2] targeted therapies including endocrine or anti-HER2 therapies are ineffective, and chemotherapy remains the only effective treatment option for TNBC in clinical practice,[3] while the prognosis remains poor. As a result, there is an urgent need for new methodologies to treat TNBC. Several studies have indicated that patients

Received: 6 December 2022
Accepted: 13 April 2023
Published: 19 April 2023

Graphical Abstract

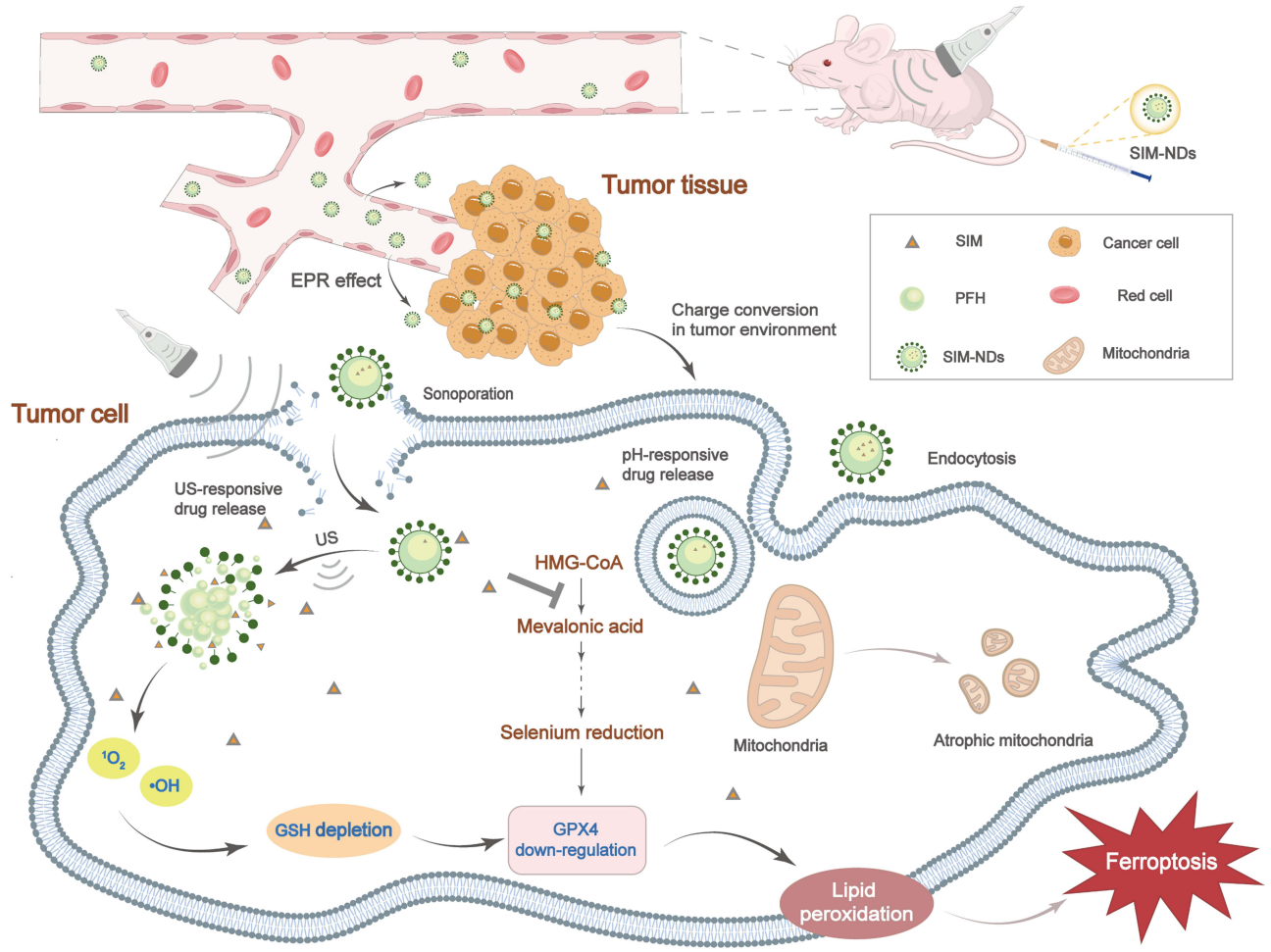

with TNBC are more delicate to ferroptosis treatment,[4,5] and numerous studies have verified that ferroptosis could effectively hinder TNBC growth.[6–8]

Ferroptosis, with the ability to effectively eliminate tumor cells, is an iron-dependent regulated cell death characterized by excessive accumulation of lipid peroxides.[9,10] Glutathione peroxidase 4 (GPX4), a key inhibitor of ferroptosis in cancer cells, is essentially a selenoprotein that detoxifies lipid peroxides by using reduced glutathione (GSH) as a cofactor.[11] In addition, there is a negative correlation between high GPX4 expression levels with the prognosis of breast cancer patients.[12] Thus, inhibiting intracellular GPX4 expression triggers ferroptotic death in cancer cells while enhancing patient prognosis.

Simvastatin (SIM) is a clinically utilized lipid-lowering medicine and a well-known inhibitor of the mevalonate (MVA) pathway with additional anticancer effects, in accordance with clinical trial results.[13,14] The MVA pathway modulates ferroptosis development by modulating the maturation of selenocysteine tRNA.[15] Therefore, SIM can lower GPX4 synthesis by blocking the MVA pathway, which can thereby initiate ferroptosis. However, poor water solubility and quick elimination of orally administered free SIM prevent its delivery to the tumor site at appropriate concentrations and reduce its bioavailability.[16,17] At the same time, long-term use can result in statin-associated muscular symptoms, new-onset type 2 diabetes, and hepatic and renal damage.[18,19] Therefore, it is critical to develop technical tools that can improve drug efficacy while decreasing the risk of side effects.

Nanocarriers have been developed as an emerging platform for more effective diagnosis and treatment of a range of diseases and provide a promising solution to the above-mentioned problems. Recently, numerous studies on the application of nanocarriers in ferroptosis have been published, with significant tumor suppressive effects.[20–22] However, a range of biological barriers may result in relatively low delivery efficiency, which can limit site-specific bioavailability and prevent appropriate therapeutic consequences.[23] Considering the poor effectiveness of nanocarriers in penetrating biological barriers, nanoscale ultrasound contrast agents (UCAs) have shown great promise in cancer therapy. UCAs perform ultrasound (US) contrast imaging by the liquid-gas phase transition and improve the permeability of the biological barrier in the presence of ultrasound-targeted microbubble disruption (UTMD).[24–26] In addition, UTMD can cause cellular damage by increasing intracellular reactive oxygen species (ROS) and depleting intracellular GSH.[27,28] However, till the present, there are few studies on the application of UCAs in ferroptosis.

To induce the ferroptosis process more efficiently and improve the ability to kill tumor cells, we designed SIM-loaded nanodroplets (NDs) with dual responsiveness (ie, US-responsive and pH-responsive) to enhance the specific aggregation of NDs in tumor tissues and can also achieve contrast-enhanced ultrasound imaging (CEUI) under the effect of US irradiation. In addition, SIM-NDs enhanced drug penetration in tumor tissues under the action of US, and then SIM and UTMD reduce selenocysteine and GSH (the two components on which GPX4 depends to function), respectively. Moreover, this combination strategy synergistically promoted the onset of the ferroptosis process, ultimately achieving inhibition of tumor progression. Our results could demonstrate that combination therapy has the potential to be a highly effective antitumor therapy and also promises to provide a novel therapeutic technological tool for the application in ferroptosis treatment of tumors.

Materials and Methods

Materials

SIM and lecithin were provided by Macklin (Shanghai, China). O-carboxymethyl chitosan (O-CMC) was supplied by Santa Cruz (TX, USA). Perfluorohexane (PFH) was achieved from Aladdin (Shanghai, China). Tween 20 was supplied by Solarbio (Beijing, China). Mevalonic acid was achieved from Sigma-Aldrich (St Louis, MO, USA). ROS inhibitor (NAC) was obtained from Beyotime (Shanghai, China). Matrigel was achieved from Corning (New York, USA). An anti-GPX4 antibody was supplied by Abcam (Cambridge, UK). An anti-GAPDH antibody was supplied by BOSTER (Wuhan, China). Anti-Ki67 antibody was supplied by Servicebio (Wuhan, China).

The Cell Culture Experiments in vitro

The triple-negative breast cancer (TNBC) cell line MDA-MB-231 was originally obtained from ScienCell (California, USA) and was incubated in DMEM medium containing 10% fetal bovine serum (FBS) and 1% penicillin/streptomycin at 37 °C in a humidified incubator containing 5% CO2. The cell experiments were classified into the following groups: Control, NDs, NDs+US, SIM, SIM-NDs, and SIM-NDs+US. (SIM concentration: 5μg/mL, The concentration of NDs was 20 μg/mL, and the concentration of SIM-NDs was 20 μg/mL. US irradiation: 0.5 W cm-2, 60s, 1.0 MHz.)

The Tissue Culture Studies Using Animal Models

Animal experiments were approved by the Research Ethics Committee of Qilu Hospital of Shandong University. Female BALB/c nude mice (4–5 weeks) were supplied by GemPharmatech (Jiangsu, China). The BALB/c nude mice were given unlimited water and food and were also subjected to a daily circadian rhythm of 12 h of light and 12 h of darkness. The tumor model was constructed by injecting MDA-MB-231 cell suspension (2×10^7) with matrigel into the right back of BALB/c nude mice.

The Preparation of Nanodroplets and Simvastatin-Loaded Nanodroplets

The emulsion homogenization technique was applied to prepare NDs or SIM-NDs. PFH, Tween 20, and lecithin were added to double-distilled water and were sonicated at 100 W for 5 min (10s working and 10s resting alternately) using an ultrasonic cell crusher (UP-250, Scientz, China). Subsequently, an aqueous solution of O-CMC with or without SIM was added dropwise to the above system. Then, it was sonicated once more for 5 min (the same parameters as above). Next, the mixture was centrifuged for 5

min at 300 rpm. After gathering it, the intermediate layer was spun at 12,500 rpm for 10 min. NDs or SIM-NDs were the precipitates. For later usage, the obtained NDs or SIM-NDs were washed with PBS for 3 times to remove free SIM and impurities. At the same time, the purifications of NDs or SIM-NDs were thoroughly mixed in PBS and stored at −20 °C.

The Characterization of Simvastatin-Loaded Nanodroplets

The morphology of SIM-NDs was evaluated using transmission electron microscopy (TEM; JEM-1400FLASH, JEOL, Tokyo, Japan). The hydrodynamic particle size and zeta potential of SIM-NDs were determined using Dynamic Light Scattering (DLS) (Zetasizer-Nano-ZS, Malvern, UK).

A UV-vis spectroscope (DS-11+Spectrophotometer, DeNovix, Wilmington, USA) operating at 238 nm was used to calculate the entrapment efficiency (EE) and loading efficiency (LE) of SIM in SIM-NDs. The formulas are as follows: EE = Mass of SIM in NDs/Mass of SIM provided × 100%; LE = Mass of the SIM in NDs/Total mass of SIM-NDs × 100%.

The dialysis approach was adopted for investigating the drug release profiles from SIM-NDs. To determine the pH responsiveness, 2 mL of SIM-NDs solution was placed in dialysis bags (molecular weight cut-off 3500, Sigma, MO, USA), and incubated in PBS buffer (50 mL) with two different pH values (pH 6.5 and pH 7.4). At various time intervals, 1 mL of the solution was taken and replaced with an equal amount of PBS. The amount of SIM released was determined by UV–vis spectroscope. SIM cumulative release (%) = the amount of SIM released/ the amount of SIM encased in SIM-NDs × 100%. In addition, the US-responsive release profile was performed by dispersing SIM-NDs with or without US irradiation in dialysis bags, with subsequent treatments as described above.

The Cellular Uptake Ability of Simvastatin-Loaded Nanodroplets

Cells were seeded in 24-well plates and cultured with a medium containing DiI-labeled SIM-NDs. After 30 minutes, one group of cells was treated with US irradiation. Cells were washed and fixed. US-responsive uptake of SIM-NDs by cells was evaluated by fluorescence microscopy (Eclipse Ti2, Nikon, Tokyo, Japan) and flow cytometry (FCM) (CytoFLEX S, Beckman, USA).

To assess the pH-responsive uptake of SIM-NDs by cells, DiI-labeled SIM-NDs dispersed at different pH (pH 6.5 and pH 7.4) were then co-cultured with cells in serum-free medium with different pH (pH 6.5 and 7.4) for 2 h. Subsequent operations were carried out as previously mentioned.

Contrast-Enhanced Ultrasound Imaging of Simvastatin-Loaded Nanodroplets

SIM-NDs sample solutions were injected into latex glove fingertip examination models, which were then immersed in a 37°C water bath, followed by CEUI to assess the ultrasound capacity of SIM-NDs. Following the administration of anesthesia to BALB/c nude mice bearing tumors, CEUI was performed in vivo. BALB/c nude mice bearing tumors were injected 200 μL of SIM-NDs or PBS through the tail vein and sonicated. Then, the US probe was positioned on the tumor's surface. A clinical ultrasound system (LOGIQ E9; GE, USA) and a 9L linear transducer were used.

Western Blotting

Intracellular proteins were extracted after MDA-MB-231 cells were subjected to various treatments for 24 h. SDS-PAGE was used to separate the proteins, which were then transferred to PVDF membranes. Based on the molecular weight of the protein, the membrane is sliced to the appropriate width. The primary antibody was incubated overnight at 4 °C, followed by the secondary antibody the next day. Then, the bands were observed using chemiluminescence equipment.

Transmission Electron Microscope Imaging of Simvastatin-Loaded Nanodroplets

After receiving various treatments for 24 h, MDA-MB-231 cells were collected, added to 2.5% glutaraldehyde fixative, and placed at 4 °C for over 4 h. After removing the fixative, it was replaced with 2% osmium tetroxide. Finally, TEM observations of ultrathin slices were made (JEM-1200EXII, JEOL, Tokyo, Japan).

The Levels of Intracellular Lipid Peroxidation in Various Treatments

After each group of cells received different treatments for 24 h, a lipid peroxidation assay (LPO) kit (Beyotime, Shanghai, China) was used following the instructions, aiming to measure the relative concentration of malondialdehyde (MDA) in the cell lysate.

The cells were planted in 12-well plates and subjected to various treatments for 24 h. The above cells were stained with the BODIPY C11 probe (Thermo Fisher, MA, USA). Finally, all the cells were digested, washed, and analyzed for FCM measurement (FACSCalibur, BD Biosciences, USA). The above-mentioned cells were also fixed and observed by fluorescence microscopy (Eclipse Ni, Nikon, Tokyo, Japan).

The Levels of Intracellular Reactive Oxygen Species Production in Various Treatments

Cells were seeded in 12-well plates and then subjected to different treatments for 24 h. Then, cells were stained for 30 minutes with a DCFH-DA probe (Beyotime, Shanghai, China), washed with PBS, analyzed by FCM, and observed by fluorescence microscopy.

The Level of Intracellular Glutathione in Various Treatments

Intracellular GSH levels were measured using a GSH assay kit (Solarbio, Beijing, China). The cells were planted in 6-well plates and incubated with various treatments for 24 h. The cells were digested, washed and collected, and processed following the steps in the instructions. Finally, using a microplate reader, the absorbance of each well was determined at 412nm (Infinite M200, TECAN, Switzerland).

In vitro Antitumor Ability of Simvastatin-Loaded Nanodroplets

The cell viability was determined based on the cck-8 kit. MDA-MB-231 cells were seeded in 24-well plates and given different treatments to incubate for 24 h. Then, DMEM medium containing 10% cck8 solution was configured to replace the original medium and incubated in the incubator. Then, a microplate reader was used to measure the absorbance of each well at 450 nm.

The Cell-light Edu Apollo 488 kit was used to assess cell proliferation capability (RiboBio, Guangzhou, China). Cells were seeded in 6-well plates, subjected to different treatments, and incubated for 24 h. Cells were digested and collected, replanted in 96-well plates overnight, labeled, fixed, and stained in the sequence of steps in line with the instructions, and photographed under a fluorescent microscope.

Transwell assays were used to analyze the migration and invasion abilities of TNBC cells. MDA-MB-231 cells were seeded on 6-well plates and subjected to different treatments for 24 h. 3×10^4 cells were harvested and planted into the upper chamber with or without matrigel. The lower chamber was filled with DMEM medium containing 15% FBS. After 24 h incubation, the transwell chambers were fixed and stained with crystal violet. Finally, the upper layer of cells was gently swabbed. The migrating or invading cells were observed and photographed under a microscope (NEXCAM-T5, Nexcope, China) and photographed. Using Image J, the migrating or invading cells were counted.

In vivo Biodistribution of Simvastatin-Loaded Nanodroplets

Once the tumor volume achieved the appropriate size, the BALB/c nude mice were randomly divided into five groups. 200μL of DiI-labeled SIM-NDs were subsequently intravenously injected into each group at various intervals (0h, 18h, 20h, 22h, 23h). Their major organs (heart, liver, spleen, lungs, and kidneys) and malignancies were gathered at 24 h for fluorescence imaging using the IVIS spectrum image system (PerkinElmer, Waltham, MA, USA).

In vivo Biosafety of Simvastatin-Loaded Nanodroplets

The healthy BALB/c nude mice (n = 3 mice per group) were intravenously injected with PBS, NDs, SIM, and SIM-NDs. The mice were sacrificed after 24 h of injection and collected blood samples. Four groups of blood samples were adopted for detecting IL-6 and TNF-α. Blood samples from PBS and SIM-NDs groups were tested different biochemical indicators using Chemray 800 Automatic Biochemical analyzer (China), including alanine aminotransferase (ALT), aspartate aminotransferase (AST), albumin (ALB), blood urea nitrogen (BUN) and creatinine (CRE).

In vivo Antitumor Ability of Simvastatin-Loaded Nanodroplets

The BALB/c nude mice were randomly allocated to 6 groups (n = 5) and administered various treatments on days 3, 6, 9, and 12 when the tumor volumes reached approximately 100–150 mm^3. The various therapies were PBS, NDs, NDs+US, SIM, SIM-NDs, and SIM-NDs+US. (SIM concentration: 5 mg/kg, the concentration of NDs was 2 mg/mL, and the

concentration of SIM-NDs was 2 mg/mL.) Nude mice were treated with or without US irradiation (1.5 W cm-2, 1 min, 1.0 MHz) after tail vein injection. Every two days, body weights and tumor volumes were recorded. The tumor volume = 0.5 × width^2 × length. In addition, major organs and subcutaneous tumor tissues were taken on day 14 for hematoxylin and eosin (HE), immunohistochemistry (IHC), and TUNEL staining.

Statistical Analysis

All experiments were performed in triplicate. The results are presented as the means ± SD. Statistical analysis was performed with GraphPad Prism 8 software. Data from numerous groups were analyzed using one-way ANOVA, and comparisons between two groups were explored using the Student's *t*-test. *$p < 0.05$, **$p < 0.01$, ***$p < 0.001$ and ****$p < 0.0001$.

Results and Discussion

Characterization of Simvastatin-Loaded Nanodroplets

Using the method of previous studies, (SIM-) NDs with O-CMC shell and PFH core with or without SIM were successfully prepared using the homogenization/emulsification method (Figure 1A).[29] TEM images showed spherical-like morphology for SIM-NDs. In neutral conditions, SIM-NDs had a recognizable core-shell structure (Figure 1B).

Under the neutral condition, the average particle size of NDs was 284.77nm, the polydispersity index (PDI) was 0.183, and the zeta potential was −7.74mV (Figure 1D). The particle size distribution of SIM-NDs at various pH levels was shown in Figure 1E. At pH 7.4 (pH of blood circulation), the average particle size of SIM-NDs was 286.19 nm, and

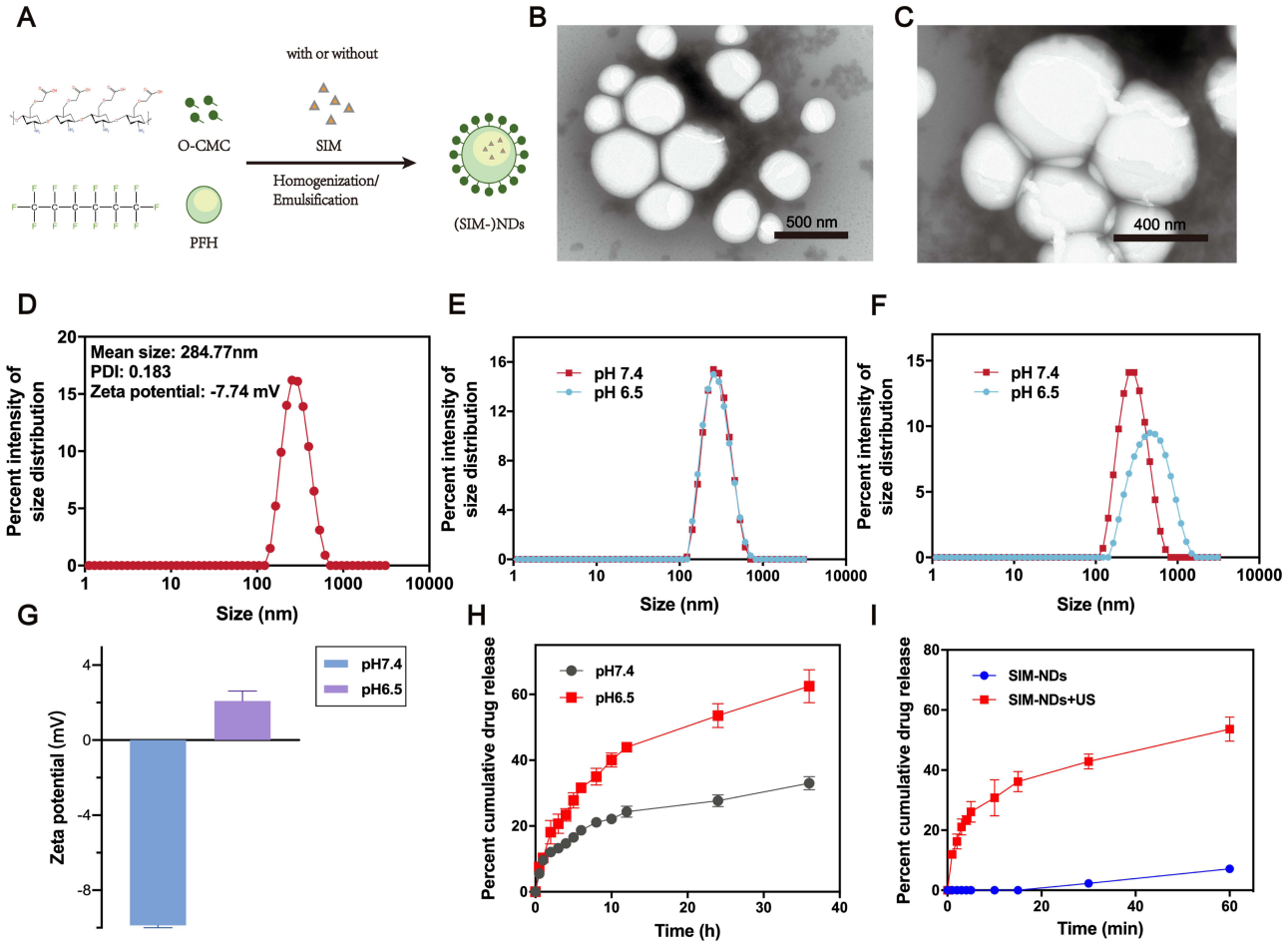

Figure 1 Characterization of SIM-NDs. (**A**) (SIM-) NDs synthesis diagram. (**B**) TEM image of SIM-NDs at pH 7.4. Scale bar: 500 nm. (**C**) TEM image of SIM-NDs at pH 6.5. Scale bar: 400 nm. (**D**) Particle size distribution of NDs. (**E**) Particle size distribution of SIM-NDs under various pH levels for 0.5 h. (**F**) Particle size distribution of SIM-NDs under various pH levels for 2 h. (**G**) Zeta potentials of SIM-NDs at various pH levels. (**H**) The drug release profiles under various pH levels. (**I**) The drug release profiles when exposed to ultrasound. All results represent the means ± SD (n = 3).

the PDI was 0.217. The loading of SIM-NDs made no significant effect on the basic characteristics of NDs. The particle size of SIM-NDs remained practically unaltered when incubated at pH 6.5 (pH of the tumor microenvironment) and pH 7.4 for 0.5 h, indicating that SIM-NDs could remain stable in the blood circulation and tumor microenvironment within a short period of time. Due to their small diameter and favorable stability, SIM-NDs could readily exude through the endothelium of tumor tissue and accumulate locally through enhanced permeability and retention (EPR) effects.[30] After incubation at pH 6.5 and pH 7.4 for 2 h, the particle size of nanodroplets remained stable at pH 7.4. Nevertheless, the particle size of SIM-NDs increased in comparison with that under the neutral condition. The increase of particle size and PDI indicated that NDs could begin to swell and aggregate (Figure 1F). This conforms to the results of TEM images under different pH conditions (Figure 1C).

The zeta potential of SIM-NDs at the neutral condition is -(9.87±1.00) mV. At the condition of pH 6.5, the zeta potential was converted from negative to positive (Figure 1G). The negative charge on the surface could allow SIM-NDs to circulate in the blood circulation for a long period, whereas the charge conversion of SIM-NDs could allow them to bind to the electrostatic attraction of tumor cells.[31,32]

Based on the data provided in Supplementary Table 1, we chose formulation 3 as the preparation scheme of SIM-NDs. The EE and LE of SIM were 77.59±0.03% and 23.87±0.01%, respectively. We measured the release profiles under different pH conditions and US irradiation. As displayed in Figure 1H, the cumulative drug release under the neutral condition for 24 h was 27.67%, which was lower than that under the acidic condition (53.58%) ($p<0.05$). This demonstrates that SIM-NDs could lower drug release in non-tumor tissues and reduce side effects. In addition, we evaluated the effect of US irradiation on drug release. After US irradiation, SIM initially exhibited an instant release, and the cumulative drug release could reach 36.18% at 15 min, and then maintained a sustained release, reaching a cumulative drug release of 53.65% at 60 min. It proves that SIM-NDs can achieve an instant release of drugs in a short period under US irradiation and then maintain a sustained release (Figure 1I).

In summary, the obtained results indicate that the nanodroplets could achieve targeted delivery to tumor sites under pH and ultrasound stimulation, which shows the potential to be a vehicle to achieve precise tumor treatment.

The Tumor-Binding Ability of Simvastatin-Loaded Nanodroplets

As shown in Figure 2A and B, S1A, the internalized uptake of SIM-NDs by cells was significantly enhanced at pH 6.5 (tumor microenvironment) than that at pH 7.4 (blood circulation). This phenomenon may be associated with the charge conversion of SIM-NDs in the tumor microenvironment, then binding to the electrostatic attraction of tumor cells. This consequently enhances the uptake of SIM-NDs by tumor cells. NDs can be internalized by cells through passive phagocytosis and sonication-mediated cavitation.[33] SIM-NDs marked with Dil are shown as red dots and nuclei marked with DAPI as blue dots. Clearly, the internalization of SIM-NDs by tumor cells is greatly enhanced after US irradiation, which was in consistence with FCM results (Figure 2C and D, S1B). This represented US irradiation can effectively enhance the intracellular uptake of nanodroplets, which might be correlated with US-mediated acoustic pore effect.[34]

We further investigated the biological distribution of SIM-NDs in BALB/c nude mice. As shown in Figure 2E, the fluorescence signal was accumulated in the tumor tissue, which might be related to the EPR effect and the charge conversion of SIM-NDs in the tumor microenvironment. The fluorescence signal was still detectable in the tumor tissue 24 h after injection, showing sustained retention of SIM-NDs in the tumor tissue. The strongest accumulation in tumor tissues was observed 2 h after injection by quantifying the average radiant efficiency (Figure 2F). In addition, the fluorescent signal was observed in the liver, which might be related to the phagocytosis of NDs by the reticuloendothelial system. Taken together, SIM-NDs could exhibit the excellent ability to accumulate in tumor tissues in vitro and in vivo.

Contrast-Enhanced Ultrasound Imaging of Simvastatin-Loaded Nanodroplets

To confirm the ultrasonographic capability of SIM-NDs, CEUI was performed separately. As shown in Figure 3A, SIM-NDs exhibited good echogenicity in CEUI mode compared to PBS. In vivo, the echogenicity of SIM-NDs in the tumor region was observed by US imaging. After intravenous injection of PBS, the tumor exhibited almost no echogenic signal, while after intravenous injection of SIM-NDs, the echogenic signal in the SIM-NDs group was significantly increased, which may be related to the aggregation of SIM-NDs in the tumor tissue (Figure 3B). SIM-loaded nanodroplets can be utilized for tumor imaging,

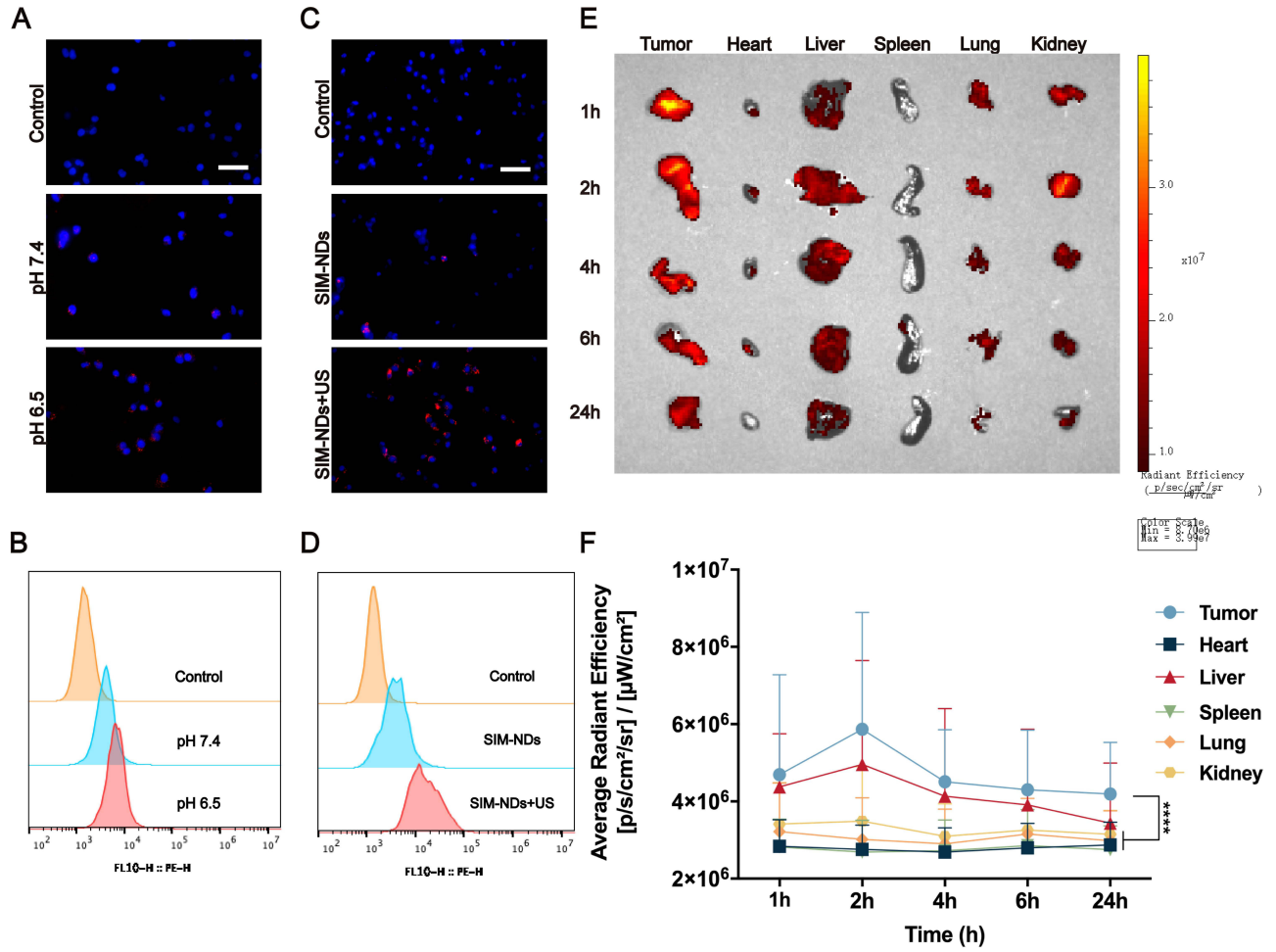

Figure 2 The tumor-binding ability of SIM-NDs. (**A**) Uptake of Dil-labeled SIM-NDs by cells under different pH conditions. Scale bar: 100μm. (**B**) Uptake of Dil-labeled SIM-NDs by cells under different pH conditions analyzed by FCM. (**C**) Uptake of Dil-labeled SIM-NDs by cells under US irradiation. Scale bar: 100μm. (**D**) Uptake of Dil-labeled SIM-NDs by cells under US irradiation analyzed by FCM. (**E**) Biodistribution of Dil-labeled SIM-NDs in BALB/c nude mice at different time intervals. (**F**) Quantitative analysis of the average radiant efficiency from D. Compared to the normal group (except for the liver group). All results represent the means ± SD (n = 3). ****p<0.0001.

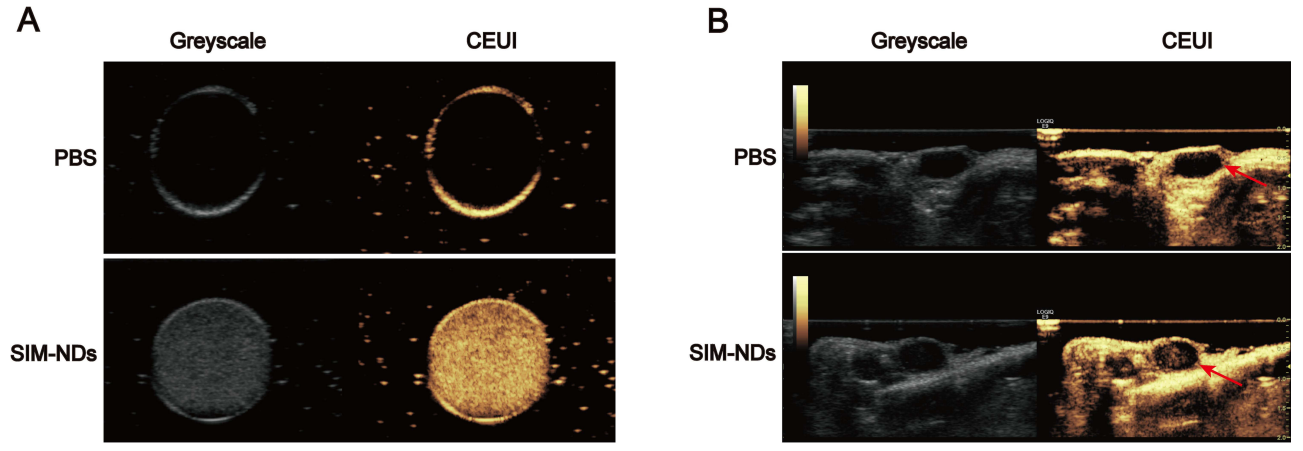

Figure 3 CEUI of SIM-NDs. (**A**) CEUI of SIM-NDs in vitro. (**B**) CEUI of SIM-NDs in vivo. The red arrow indicates the position of the tumor.

tumor treatment, and therapeutic efficacy evaluation at the same time, combining diagnostic and therapeutic applications. To conclude, SIM-NDs have excellent ultrasound contrast imaging ability and may have the capability of visualizing the treatment.

Ultrasound-Targeted Microbubble Disruption Combined with Simvastatin-Loaded Nanodroplets Initiate Ferroptosis

The ultrastructural morphological changes of ferroptosis at the cellular level are different from apoptosis, necrosis, and autophagy. The morphological changes of ferroptosis are mainly characterized by smaller mitochondrial volume, increased membrane density, and reduced or absent mitochondrial cristae.[4] Therefore, we observed the morphological alterations of cellular mitochondria under transmission electron microscopy. As shown in Figure 4A, compared with normal cells, mitochondria in the NDs group were mildly swollen and mitochondrial cristae were visible. By contrast, the NDs+US group showed smaller mitochondrial volume and increased membrane density, indicating that it was the combined effect of UTMD rather than NDs alone that could initiate ferroptosis. Only a few mitochondria in the SIM and SIM-NDs groups

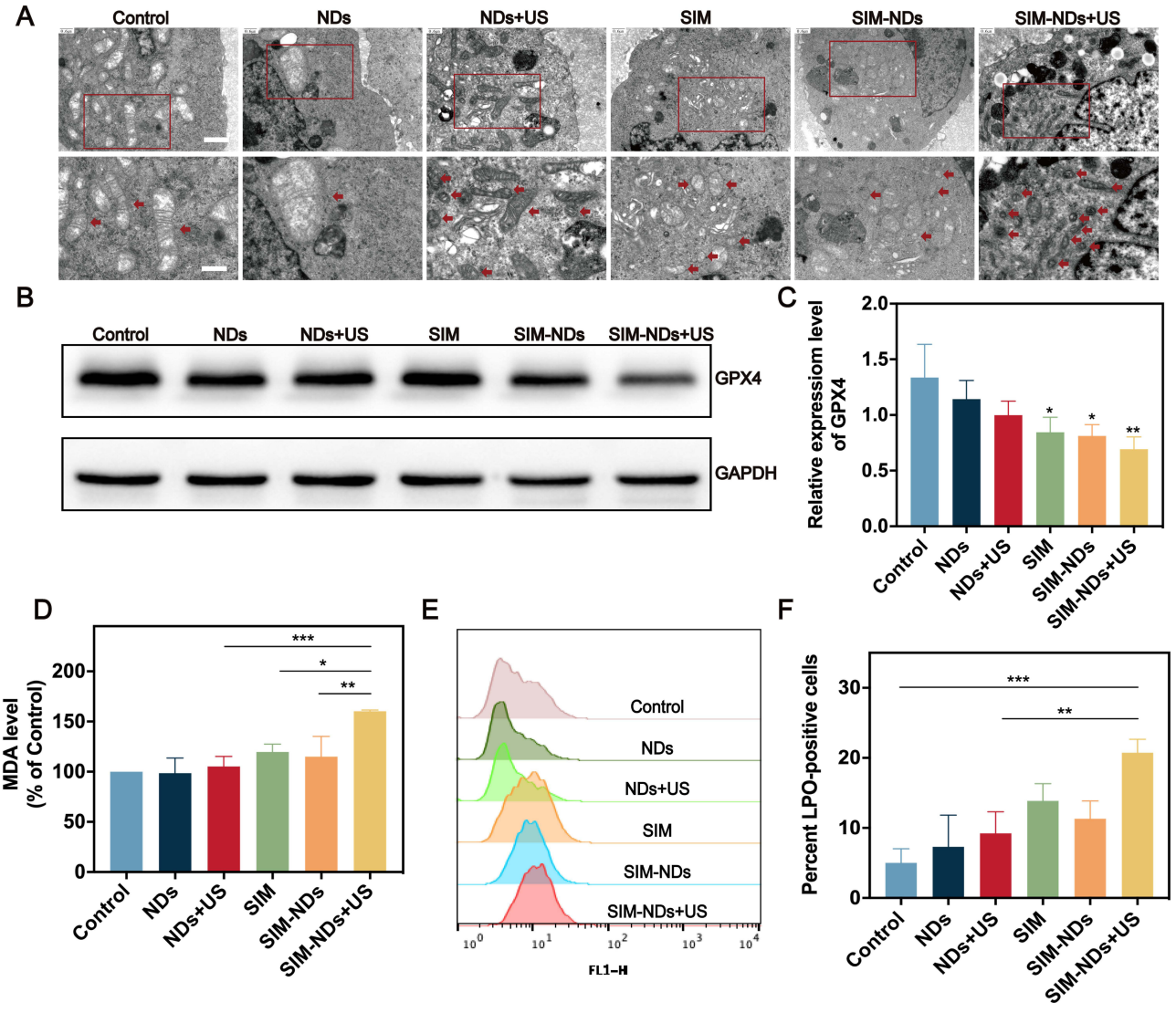

Figure 4 UTMD combined with SIM-NDs initiates ferroptosis. (**A**) TEM images of TNBC cells after various therapies. The bottom figures (magnification 2X) are enlarged views of the red boxes in the above figure, respectively. The red arrows represent the mitochondria in the cells. Scale bar: 1.2 μm, 0.6 μm. (**B**) The relative expression level of GPX4 on MDA-MB-231 cells with various treatments. (**C**) Quantification of GPX4/GAPDH was performed from B using Image J. Compared to the normal group. (**D**) MDA levels of breast cancer cells after different treatments. (**E**) Lipid peroxidation levels of MDA-MB-231 cells after various treatments were quantified by FCM. (**F**) The percentage of positive cells was obtained from E using Flowjo. All results represent the means ± SD (n = 3). *p<0.05, **p<0.01, ***p<0.001.

became smaller in size and increased in membrane density, whereas most mitochondria in the SIM-NDs+US group became significantly smaller in size and increased in membrane density, revealing the typical morphological changes of ferroptosis.

Blocking intracellular antioxidant enzymes can disrupt the balance between oxidative damage and antioxidant defense, thereby initiating ferroptosis. As a central suppressor of ferroptosis in cancer cells, GPX4 can fight against lipid peroxidation and reduce toxic lipid peroxides to non-toxic lipid alcohols.[11] We extracted proteins from the differently treated cells and performed Western blotting (Figure 4B). The expression levels of GPX4 were differentially downregulated in the NDs+US, SIM, and SIM-NDs groups in relative to the normal group. In addition, due to the synergistic effect of intracellular SIM aggregation and UTMD, the decrease in GPX4 expression levels was most pronounced in the SIM-NDs+US group ($p<0.01$) (Figure 4C).

As previously mentioned, ferroptosis is essentially an excessive accumulation of lipid peroxidation, which results in cellular damage.[35] Then, we verified the levels of lipid peroxidation in different groups. MDA is a natural product of cellular lipid oxidation. As expected, the NDs+US group had slightly elevated MDA levels, and both the SIM and SIM-NDS groups had different levels of elevation. Compared to the other groups, MDA levels were significantly increased in the SIM-NDs+US group (Figure 4D). The results of the FCM data and fluorescence images of lipid peroxidation were consistent with those for MDA levels (Figure 4E and F, S2), further confirming that the combined treatment could successfully initiate ferroptosis.

Collectively, the above results provide strong evidence that the combination treatment of SIM-NDs and UTMD could synergistically initiate the ferroptosis process, which causes cellular damage.

The Mechanism of Ferroptosis Induced by Ultrasound-Targeted Microbubble Disruption Combined with Simvastatin-Loaded Nanodroplets

After we demonstrated that the combined therapeutic approach can synergistically induce ferroptosis, the mechanism of ferroptosis induction by SIM-NDs in combination with UTMD was further evaluated. As a central inhibitor of ferroptosis in cancer cells, the intracellular expression of GPX4 is largely dependent on GSH and selenium.[11]

As reported, UTMD can disrupt the redox balance in cancer cells by elevating intracellular ROS. Moreover, the increase of intracellular ROS levels can scavenge GSH.[27,28,36–38] As displayed in Figure 5A and B, the most significant change of ROS level was observed in the SIM-NDs+US group, followed by the NDs+US group. The US group (ie, NDs +US group, SIM-NDs+US group) produced more ROS than the SIM group (ie, SIM group, SIM-NDs group). The fluorescence microscopy results were also in consistence (Figure 5D).

The changes in intracellular GSH content were consistent with expectations and were inversely associated with ROS levels (Figure 5C). The SIM and SIM-NDs groups had high levels of GSH than the US group (ie, NDs+US group, SIM-NDs+US group), and the SIM-NDs+US group had the highest GSH depletion ($p<0.0001$).

Based on the above findings, the relationship between UTMD and GPX4 was further investigated. After the addition of ROS inhibitor (NAC), we found that the GSH level and the expression level of GPX4 were restored to be comparable to the control group (Figure 5E–G). In conclusion, the results suggested that UTMD could down-regulate GPX4 expression via the ROS/GSH/GPX4 pathway.

SIM, a classical HMG-CoA reductase (HMGCR) inhibitor, can mediate cancer cytotoxicity by depleting MVA downstream of HMGCR in cells rather than inhibiting HMGCR per se.[39] As reported, MVA and its downstream products positively regulate selenium transport.[40] The verification was made using Western blotting. As shown in Figure 5H and I, GPX4 expression was decreased in the SIM group compared to the control group ($p<0.05$), but upregulated after MVA supplementation. However, no significant difference was found in GPX4 after the addition of NAC. To summarize the above, SIM influences GPX4 primarily by lowering the intracellular MVA level.

The combined treatment strategy could initiate ferroptosis mainly by reducing the intracellular GSH level (the effect of UTMD) and depleting the intracellular MVA content (the effect of SIM) to synergistically down-regulate GPX4, which may provide a novel perspective for the application of ferroptosis in cancer therapy.

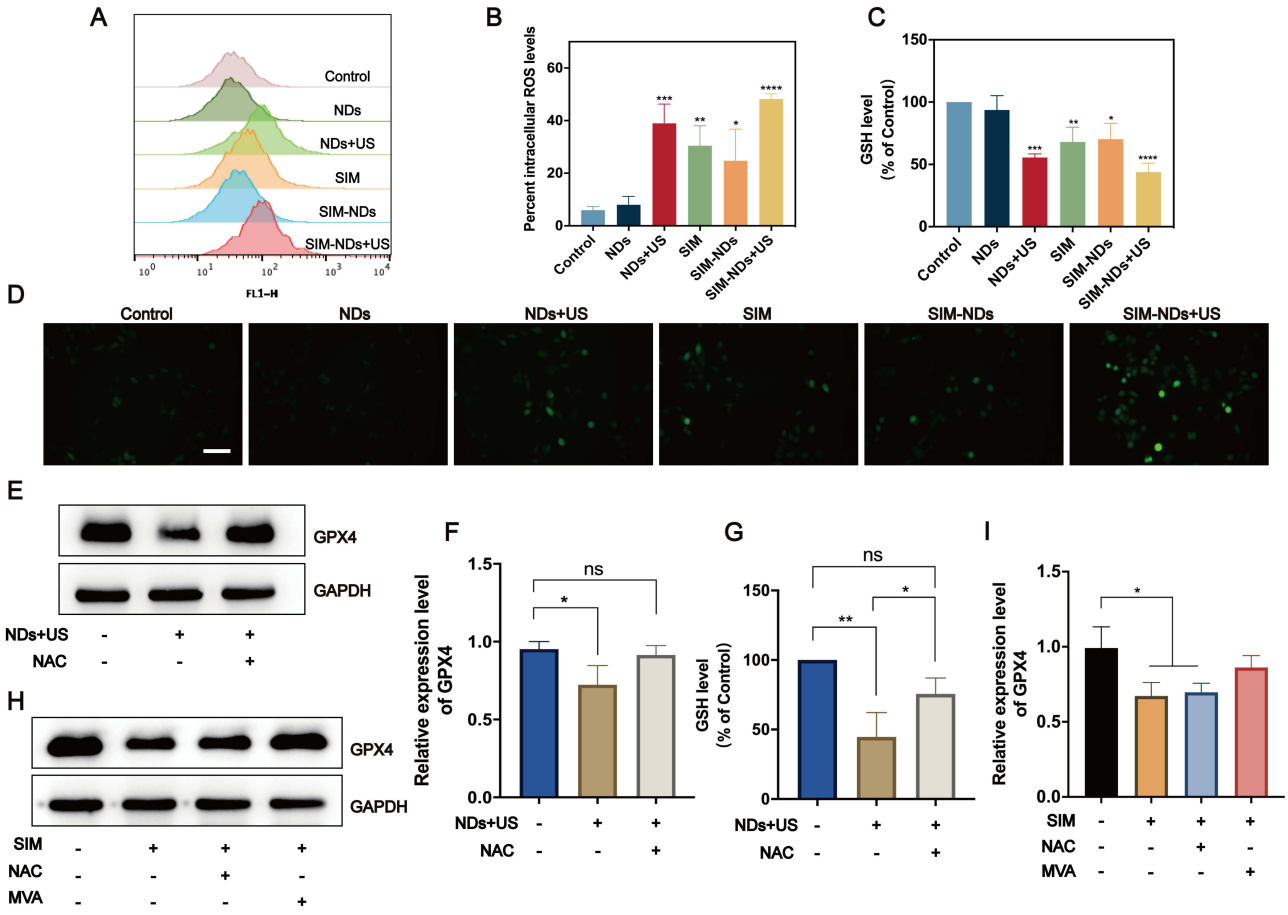

Figure 5 Mechanism of ferroptosis induced by UTMD combined with SIM-NDs. (**A**) ROS generation in MDA-MB-231 cells after different treatments were quantified by FCM. (**B**) The percentage of positive cells rate was obtained from A using Flowjo. Compared to the normal group. (**C**) Intracellular GSH content. Compared to the normal group. (**D**) Fluorescence images of ROS generation in MDA-MB-231 cells after different treatments (DCFH-DA probe staining). Scale bar: 100μm. (**E, F**) The expression level (**E**) and quantitative analysis (**F**) of GPX4 in MDA-MB-231 cells after various treatments (Control, NDs+US, NDs+US+NAC). (**G**) Intracellular GSH content with various treatments (Control, NDs+US, NDs+US+NAC). (**H** and **I**) The expression level (**H**) and quantitative analysis (**I**) of GPX4 in MDA-MB-231 cells after various treatments (Control, SIM, SIM+NAC, SIM+MVA). All results represent the means ± SD (n = 3). *p<0.05, **p<0.01, ***p<0.001, ****p<0.0001.

In vitro Antitumor Ability of Simvastatin-Loaded Nanodroplets Upon Ultrasound Irradiation

Ferroptosis makes a well-inhibiting effect on tumor growth and metastasis.[41,42] As shown in Figure 6A and B, the green dots represent cells in the proliferation phase and the blue dots represent live cells. The NDs+US group, SIM group, and SIM-NDs group exhibited varying degrees of decreased proliferation ability. The percentages of Edu-positive cells were 53.79±10.88%, 46.37±7.01%, and 53.01±2.82%. The lowest percentage of Edu-positive cells was found in the SIM-NDs +US group (32.76±7.37%) (p<0.0001).

The antitumor effect of SIM-NDs and UTMD was further evaluated by CCK-8 assay (Figure 6C). Untreated cells were used as control and exhibited 100% cell viability. Due to its excellent biocompatibility, the cell survival of the NDs group was not significantly different from those of the comparison group.[25,43] By contrast, SIM-NDs+US exhibited the lowest viability (p<0.0001). The above results displayed a similar trend to that detected in the Edu assay, suggesting that the combined treatment had more significant antitumor effects than a single treatment.

To evaluate the ability of the combined treatment strategy to inhibit tumor metastasis, the invasion and migration ability of cells was evaluated using transwell assays in vitro. The SIM-NDs+US group had the fewest migrating cells (17.00 ± 11.36), as displayed in Figure 6D and F. Comparatively, there were 118.00 ± 38.57, 59.00 ± 30.81, and 84.33 ± 28.59 migrating cells in the NDs+US, SIM, and SIM-NDs groups, respectively. As shown in Figure 6E and G, the

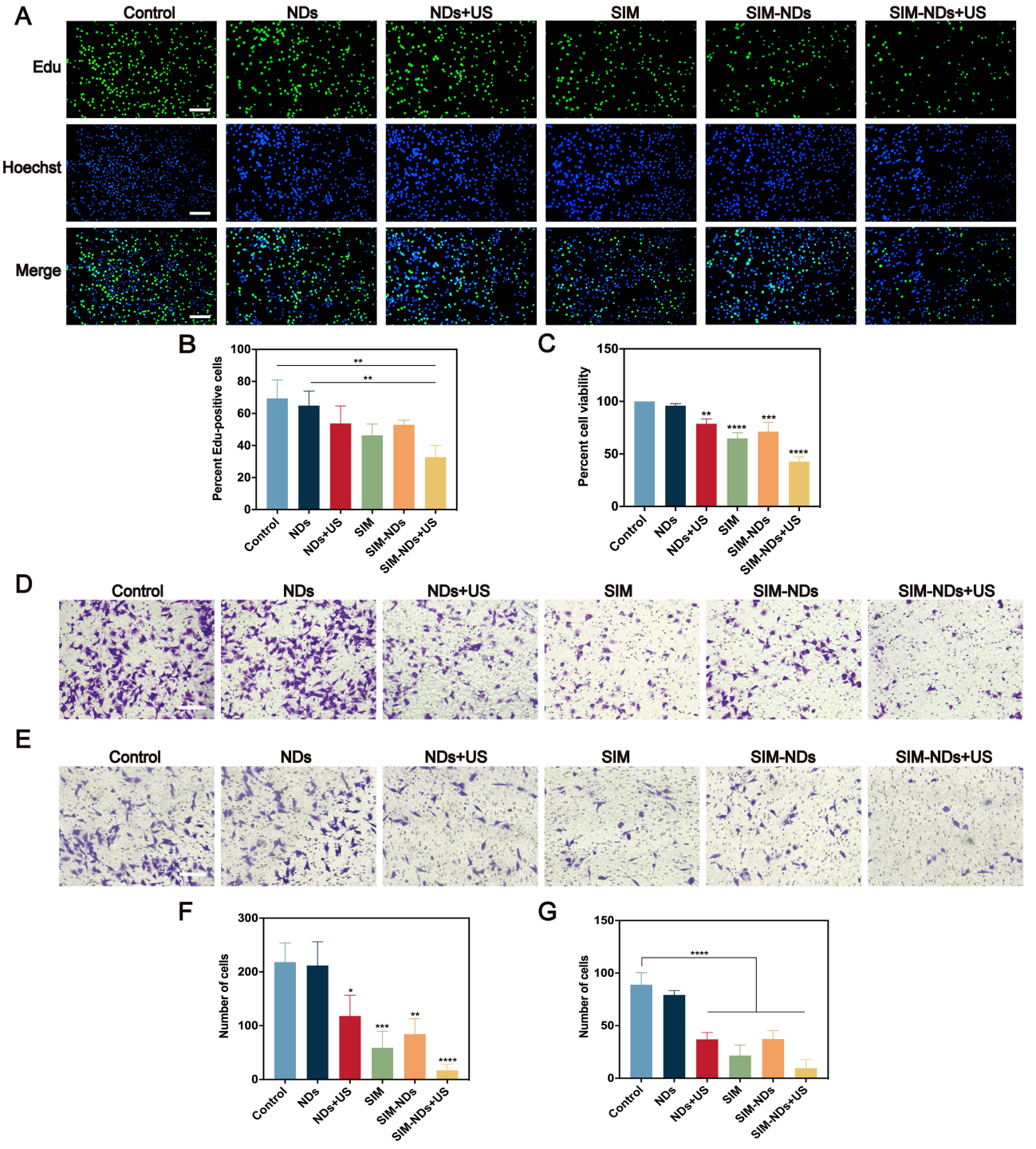

Figure 6 In vitro antitumor ability of SIM-NDs upon US irradiation. (**A**) Fluorescence images of cell proliferation ability treated for 24 h under various treatments. Scale bar: 200μm. (**B**) The percentage of Edu-positive cells was obtained from A using Image J. (**C**) Cell viability of MDA-MB-231 cells treated for 24 h under various treatments. Compared to the normal group. (**D** and **E**) Transwell migration (**D**) and invasion (**E**) experiments for 24 h of different treatment treatments. Scale bar: 200μm. (**F** and **G**) Quantification of the migrating cells (**F**) and invading cells. Compared to the normal group. (**G**) All results represent the means ± SD (n = 3). *p<0.05, **p<0.01, ***p<0.001, ****p<0.0001.

conclusions of the invasion assay were comparable to those of the migration assay. Therefore, the SIM-NDs+US group had the remarkable ability to inhibit cell invasion (p<0.0001).

These findings confirmed that combining UTMD and SIM-NDs could effectively prevent the invasion and migration of tumors.

In vivo Antitumor Ability of Simvastatin-Loaded Nanodroplets Upon Ultrasound Irradiation

Subsequently, we appraised the antitumor ability of the combination treatment in vivo. The subcutaneous tumor tissues and major organs were extracted on day 14, and the tumor tissues were photographed and weighed (Figure 7A). As shown in Figure 7B, the NDs group made almost no inhibitory effect on tumor growth compared with the negative control group. The tumor growth rate that was most slowly growing was observed in the SIM-NDs +US group, and the NDs+US, SIM, and SIM-NDs groups all had varying degrees of tumor growth inhibition potential. Tumor weight was noticeably lower observed in the SIM-NDs+US group (0.25 ± 0.10 g) compared to the SIM-NDs (0.64 ± 0.22 g) and NDs+US groups (0.75 ± 0.04 g), emphasizing the benefit of the combined therapy (Figure 7C).

After the completion of therapy, the survival rate of nude mice in each group was 100%. As shown in Figure 7D, during the treatment period, there was no appreciable difference in the body weight of the mice between groups. The biochemical parameters (ALT, AST, ALB, BUN, CRE) of the control group and SIM-NDs group were also within the normal range (p >0.05) (Figure S3). In addition, HE staining of the major organs in each group revealed no pathological changes (Figure S4), revealing that SIM-NDs have favorable biosafety and biocompatibility in vivo. However, the HE section of the lungs showed that treatment may increase the infiltration of inflammatory cells in the lungs. This may be due to the fact that NDs containing perfluorinated compounds can be exhaled in the body in the form of steam,[44,45] and thus the NDs deposit in the lungs to a certain extent, activating inflammatory cells to engulf the deposited nanodroplets to protect the body, conforming to previous studies.[46] This is consistent with the results of the biodistribution experiment

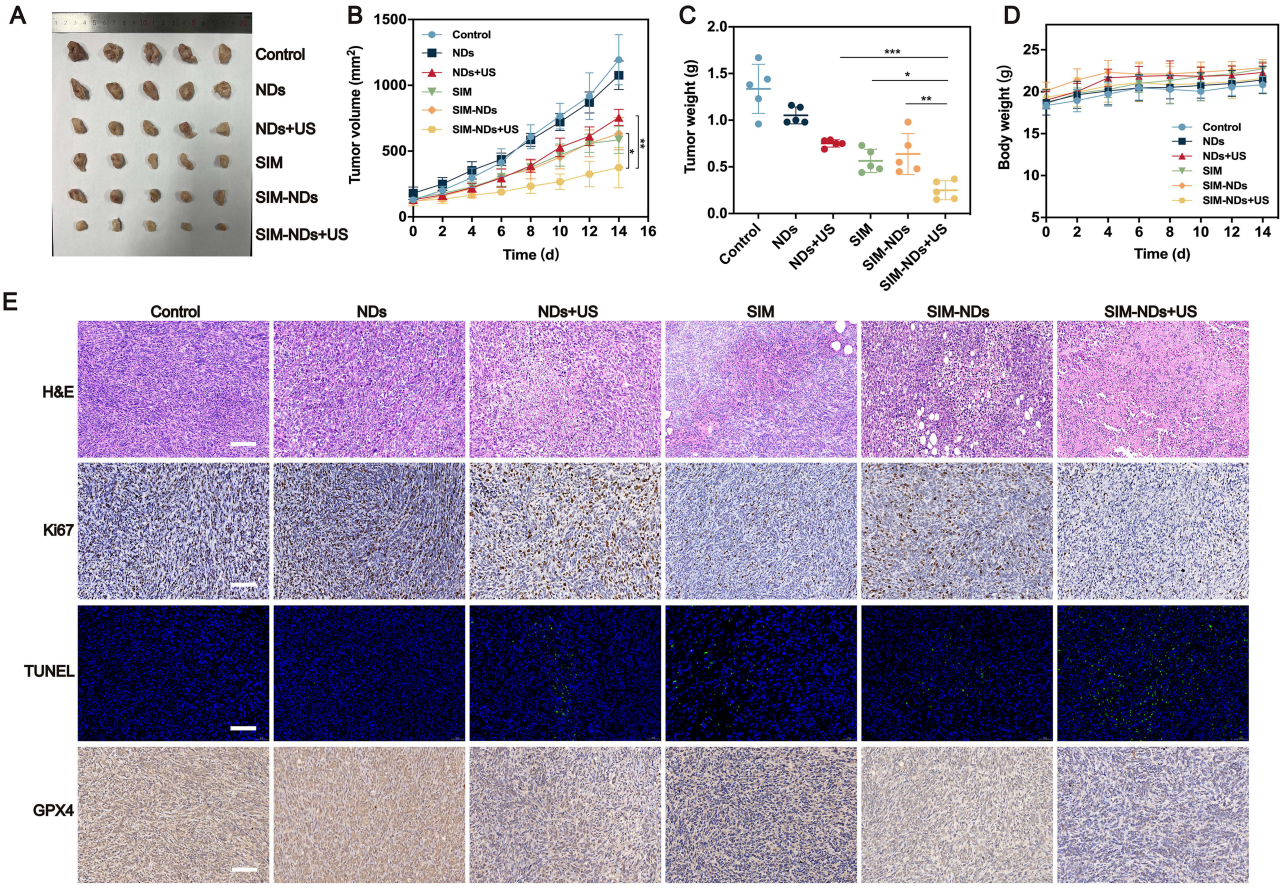

Figure 7 In vivo antitumor ability of SIM-NDs upon US irradiation. (**A**) Photographs of isolated tumors at the end of treatment. (**B**) Tumor growth profiles of various groups. (**C**) The weight of the isolated tumors in each group. (**D**) Body weight changes in mice during cancer treatment. (**E**) HE, TUNEL, and IHC staining of isolated tumors under different therapeutic modalities. Scale bar: 100 μm. All results represent the means ± SD (n = 5). *p<0.05, **p<0.01, ***p<0.001.

in vivo. In Figure 2E and F, it can be found that fewer NDs accumulate in the lung compared with the tumor tissue ($p<0.0001$), whose fluorescence signal diminishes gradually over 24 h, most likely as a result of biodegradation and removal of NDs from the body.[47] To further confirm the extent of the systemic inflammatory response, we measured IL-6 and TNF-α in serum. As shown in Figure S5A and B, we found only slight increases in IL-6 and TNF-α in the treated groups compared to the control group ($p >0.05$), indicating a very mild inflammatory response.

To further evaluate the antitumor ability, we stained the isolated tumor tissues with HE, TUNEL, and IHC staining (Figure 7E). The SIM-NDs+US group demonstrated the most evident damage, according to HE staining. TUNEL-positive apoptotic cells gave rise to green fluorescence, whereas TUNEL-negative cells exhibited blue fluorescence. The SIM-NDs+US group had the most apoptotic cells. In addition, a few apoptotic cells were seen in the NDs+US group. HE staining obtained consistent results. The IHC staining of Ki67 demonstrated cell proliferation activity, with the NDs+US group having a modestly reduced cell proliferation ability and the SIM-NDs+US group having a dramatically reduced cell proliferation ability. These outcomes matched those of the cellular assay, revealing the excellent antitumor ability of the combination therapy. In addition, IHC staining of GPX4 was performed to assess its expression within the tumor tissues. In relative to the SIM group and NDs+US group, GPX4 expression was significantly reduced in the SIM-NDs +US group. This suggests that the combined treatment would significantly down-regulate GPX4 expression in tumor tissues, consistent with the cellular assay data.

Conclusion

To conclude, in this study, we successfully fabricated a SIM-carrying nanodroplet with O-CMC as the shell and PFH as the core. SIM-NDs had favorable CEUI ability for integrated diagnosis and treatment. We found that UTMD inhibited tumor growth by initiating ferroptosis via the ROS/GSH/GPX4 axis. The combination of UTMD and SIM-NDs made a synergistic impact on the occurrence of ferroptosis. This treatment strategy could be a guideline for the translation of ferroptosis therapeutic strategy in clinical implementation. However, there are still some limitations in this study that need to be addressed, for instance, how to avoid partial deposition in the lungs caused by the NDs containing perfluorinated compounds, and the need for further studies in different cell lines and animal models.

Data Sharing Statement

The datasets used and/or analyzed during the current study are available from the corresponding author on reasonable request.

Ethics Approval and Consent to Participate

All animal experimental procedures were approved by the Research Ethics Committee of Qilu Hospital of Shandong University (Dwll-2022-047) and carried out in accordance with the UK Animals (Scientific Procedures) Act (1986).

Author Contributions

All authors made a significant contribution to the work reported, whether that is in the conception, study design, execution, acquisition of data, analysis, and interpretation, or all these areas; took part in drafting, revising or critically reviewing the article; gave final approval of the version to be published; have agreed on the journal to which the article has been submitted; and agree to be accountable for all aspects of the work.

Funding

This study was financially supported by the National Natural Science Foundation of China (No. 82071937), and the National Science Fund for Distinguished Young Scholars (No. 82102055).

Disclosure

The authors declare that they have no competing interests.

References

1. Foulkes WD, Reis-Filho JS, Reis-Filho JS. Triple-negative breast cancer. *N Engl J Med*. 2010;363:1938–1948. doi:10.1056/NEJMra1001389
2. Yu H, Yang C, Jian L, et al. Sulfasalazine-induced ferroptosis in breast cancer cells is reduced by the inhibitory effect of estrogen receptor on the transferrin receptor. *Oncol Rep*. 2019. doi:10.3892/or.2019.7189
3. Denkert C, Liedtke C, Tutt A, von Minckwitz G. Molecular alterations in triple-negative breast cancer—the road to new treatment strategies. *Lancet*. 2017;389(10087):2430–2442. doi:10.1016/S0140-6736(16)32454-0
4. Mou Y, Wang J, Wu J, et al. Ferroptosis, a new form of cell death: opportunities and challenges in cancer. *J Hematol Oncol*. 2019;12(1):34. doi:10.1186/s13045-019-0720-y
5. Doll S, Proneth B, Tyurina YY, et al. ACSL4 dictates ferroptosis sensitivity by shaping cellular lipid composition. *Nat Chem Biol*. 2017;13(1):91–98. doi:10.1038/nchembio.2239
6. Ding Y, Chen X, Liu C, et al. Identification of a small molecule as inducer of ferroptosis and apoptosis through ubiquitination of GPX4 in triple negative breast cancer cells. *J Hematol Oncol*. 2021;14(1):19. doi:10.1186/s13045-020-01016-8
7. Zhu J, Dai P, Liu F, et al. Upconverting nanocarriers enable triggered microtubule inhibition and concurrent ferroptosis induction for selective treatment of triple-negative breast cancer. *Nano Lett*. 2020;20(9):6235–6245. doi:10.1021/acs.nanolett.0c00502
8. Hou L, Pu L, Chen Y, et al. Targeted intervention of NF2–YAP signaling axis in CD24-overexpressing cells contributes to encouraging therapeutic effects in TNBC. *ACS Nano*. 2022;16(4):5807–5819. doi:10.1021/acsnano.1c10921
9. Chen X, Kang R, Kroemer G, Tang D. Broadening horizons: the role of ferroptosis in cancer. *Nat Rev Clin Oncol*. 2021;18(5):280–296. doi:10.1038/s41571-020-00462-0
10. Dixon SJ, Lemberg KM, Lamprecht MR, et al. Ferroptosis: an iron-dependent form of nonapoptotic cell death. *Cell*. 2012;149(5):1060–1072. doi:10.1016/j.cell.2012.03.042
11. Yang WS, SriRamaratnam R, Welsch ME, et al. Regulation of ferroptotic cancer cell death by GPX4. *Cell*. 2014;156(1–2):317–331. doi:10.1016/j.cell.2013.12.010
12. Zhang X, Sui S, Wang L, et al. Inhibition of tumor propellant glutathione peroxidase 4 induces ferroptosis in cancer cells and enhances anticancer effect of cisplatin. *J Cell Physiol*. 2020;235(4):3425–3437. doi:10.1002/jcp.29232
13. Bjarnadottir O, Romero Q, Bendahl PO, et al. Targeting HMG-CoA reductase with statins in a window-of-opportunity breast cancer trial. *Breast Cancer Res Treat*. 2013;138(2):499–508. doi:10.1007/s10549-013-2473-6
14. Sondergaard T, Pedersen P, Andersen T, et al. A Phase II clinical trial does not show that high dose simvastatin has beneficial effect on markers of bone turnover in multiple myeloma. *Hematol Oncol*. 2009;27(1):17–22. doi:10.1002/hon.869
15. Li J, Cao F, Liang YH, et al. Ferroptosis: past, present and future. *Cell Death Dis*. 2020;11(2):88. doi:10.1038/s41419-020-2298-2
16. Petyaev IM. State of the art paper improvement of hepatic bioavailability as a new step for the future of statin. *aoms*. 2015;2:406–410. doi:10.5114/aoms.2015.50972
17. Schachter M. Chemical, pharmacokinetic and pharmacodynamic properties of statins: an update. *Fundam Clin Pharmacol*. 2005;19(1):117–125. doi:10.1111/j.1472-8206.2004.00299.x
18. Preiss D. Risk of incident diabetes with intensive-dose compared with moderate-dose statin therapy: a meta-analysis. *JAMA*. 2011;305(24):2556. doi:10.1001/jama.2011.860
19. Rosenson RS, Baker SK, Jacobson TA, Kopecky SL, Parker BA. An assessment by the Statin Muscle safety task force: 2014 update. *J Clin Lipidol*. 2014;8(3):S58–S71. doi:10.1016/j.jacl.2014.03.004
20. Li K, Lin C, Li M, et al. Multienzyme-like reactivity cooperatively impairs glutathione peroxidase 4 and ferroptosis suppressor protein 1 pathways in triple-negative breast cancer for sensitized ferroptosis therapy. *ACS Nano*. 2022;16(2):2381–2398. doi:10.1021/acsnano.1c08664
21. Gai C, Liu C, Wu X, et al. MT1DP loaded by folate-modified liposomes sensitizes erastin-induced ferroptosis via regulating miR-365a-3p/NRF2 axis in non-small cell lung cancer cells. *Cell Death Dis*. 2020;11(9):751. doi:10.1038/s41419-020-02939-3
22. Tao W, Wang N, Ruan J, et al. Enhanced ROS-boosted phototherapy against pancreatic cancer via Nrf2-mediated stress-defense pathway suppression and ferroptosis induction. *ACS Appl Mater Interfaces*. 2022;14(5):6404–6416. doi:10.1021/acsami.1c22861
23. Degors IMS, Wang C, Rehman ZU, Zuhorn IS. Carriers break barriers in drug delivery: endocytosis and endosomal escape of gene delivery vectors. *Acc Chem Res*. 2019;52(7):1750–1760. doi:10.1021/acs.accounts.9b00177
24. Shafi AS, McClements J, Albaijan I, Abou-Saleh RH, Moran C, Koutsos V. Probing phospholipid microbubbles by atomic force microscopy to quantify bubble mechanics and nanostructural shell properties. *Colloids Surf B Biointerfaces*. 2019;181:506–515. doi:10.1016/j.colsurfb.2019.04.062
25. Shang M, Sun X, Guo L, et al. pH- and ultrasound-responsive paclitaxel-loaded carboxymethyl chitosan nanodroplets for combined imaging and synergistic chemoradiotherapy. *IJN*. 2020;15:537–552. doi:10.2147/IJN.S233669
26. Sun W, Li Z, Zhou X, Yang G, Yuan L. Efficient exosome delivery in refractory tissues assisted by ultrasound-targeted microbubble destruction. *Drug Deliv*. 2019;26(1):45–50. doi:10.1080/10717544.2018.1534898
27. Shi D, Guo L, Sun X, et al. UTMD inhibit EMT of breast cancer through the ROS/miR-200c/ZEB1 axis. *Sci Rep*. 2020;10(1):6657. doi:10.1038/s41598-020-63653-w
28. Xu Q, Zhan G, Zhang Z, Yong T, Yang X, Gan L. Manganese porphyrin-based metal-organic framework for synergistic sonodynamic therapy and ferroptosis in hypoxic tumors. *Theranostics*. 2021;11(4):1937–1952. doi:10.7150/thno.45511
29. Meng D, Guo L, Shi D, et al. Charge-conversion and ultrasound-responsive O-carboxymethyl chitosan nanodroplets for controlled drug delivery. *Nanomedicine*. 2019;14(19):2549–2565. doi:10.2217/nnm-2019-0217
30. Singh R, Lillard JW. Nanoparticle-based targeted drug delivery. *Exp Mol Pathol*. 2009;86(3):215–223. doi:10.1016/j.yexmp.2008.12.004
31. Gujarathi NA, Rane BR, Patel JK. pH sensitive polyelectrolyte complex of O-carboxymethyl chitosan and poly (acrylic acid) cross-linked with calcium for sustained delivery of acid susceptible drugs. *Int J Pharm*. 2012;436(1–2):418–425. doi:10.1016/j.ijpharm.2012.07.016
32. Kalliola S, Repo E, Srivastava V, et al. The pH sensitive properties of carboxymethyl chitosan nanoparticles cross-linked with calcium ions. *Colloids Surf B Biointerfaces*. 2017;153:229–236. doi:10.1016/j.colsurfb.2017.02.025
33. Lee JY, Carugo D, Crake C, et al. Nanoparticle-loaded protein-polymer nanodroplets for improved stability and conversion efficiency in ultrasound imaging and drug delivery. *Adv Mater*. 2015;27(37):5484–5492. doi:10.1002/adma.201502022

34. Chowdhury SM, Abou-Elkacem L, Lee T, Dahl J, Lutz AM. Ultrasound and microbubble mediated therapeutic delivery: underlying mechanisms and future outlook. *J Control Release*. 2020;326:75–90. doi:10.1016/j.jconrel.2020.06.008
35. Yan B, Ai Y, Sun Q, et al. Membrane damage during ferroptosis is caused by oxidation of phospholipids catalyzed by the oxidoreductases POR and CYB5R1. *Mol Cell*. 2021;81(2):355–369.e10. doi:10.1016/j.molcel.2020.11.024
36. Qu F, Wang P, Zhang K, et al. Manipulation of Mitophagy by "All-in-One" nanosensitizer augments sonodynamic glioma therapy. *Autophagy*. 2020;16(8):1413–1435. doi:10.1080/15548627.2019.1687210
37. He C, Zhang X, Yan R, et al. Enhancement of cisplatin efficacy by lipid–CaO_2 nanocarrier-mediated comprehensive modulation of the tumor microenvironment. *Biomater Sci*. 2019;7(10):4260–4272. doi:10.1039/C9BM00797K
38. Wei G, Huang L, Jiang Y, et al. Lenvatinib-zinc phthalocyanine conjugates as potential agents for enhancing synergistic therapy of multidrug-resistant cancer by glutathione depletion. *Eur J Med Chem*. 2019;169:53–64. doi:10.1016/j.ejmech.2019.02.065
39. Dorsch M, Kowalczyk M, Planque M, et al. Statins affect cancer cell plasticity with distinct consequences for tumor progression and metastasis. *Cell Rep*. 2021;37(8):110056. doi:10.1016/j.celrep.2021.110056
40. Jiang W, Hu JW, He XR, Jin WL, He XY. Statins: a repurposed drug to fight cancer. *J Exp Clin Cancer Res*. 2021;40(1):241. doi:10.1186/s13046-021-02041-2
41. Wei R, Zhao Y, Wang J, et al. Tagitinin C induces ferroptosis through PERK-Nrf2-HO-1 signaling pathway in colorectal cancer cells. *Int J Biol Sci*. 2021;17(11):2703–2717. doi:10.7150/ijbs.59404
42. Guan D, Zhou W, Wei H, et al. Ferritinophagy-mediated ferroptosis and activation of Keap1/Nrf2/HO-1 pathway were conducive to EMT inhibition of gastric cancer cells in action of 2,2-di-pyridineketone hydrazone dithiocarbamate butyric acid ester. *Oxid Med Cell Longev*. 2022;2022:1–15. doi:10.1155/2022/3920664
43. Wang X, Shang M, Sun X, et al. Dual-responsive nanodroplets combined with ultrasound-targeted microbubble destruction suppress tumor growth and metastasis via autophagy blockade. *J Control Release*. 2022;343:66–77. doi:10.1016/j.jconrel.2022.01.009
44. Lowe KC. Perfluorinated blood substitutes and artificial oxygen carriers. *Blood Rev*. 1999;13(3):171–184. doi:10.1054/blre.1999.0113
45. Tian F, Wang S, Shi K, et al. Dual-depletion of intratumoral lactate and ATP with radicals generation for cascade metabolic-chemodynamic therapy. *Adv Sci*. 2021;8(24):2102595. doi:10.1002/advs.202102595
46. Gosens I, Post JA, de la Fonteyne LJ, et al. Impact of agglomeration state of nano- and submicron sized gold particles on pulmonary inflammation. *Part Fibre Toxicol*. 2010;7(1):37. doi:10.1186/1743-8977-7-37
47. Xu Y, Liu S, Zeng L, et al. An enzyme-engineered nonporous copper (I) coordination polymer nanoplatform for cuproptosis-based synergistic cancer therapy. *Adv Mater*. 2022;34(43):2204733. doi:10.1002/adma.202204733